Title

A Dual-Gene Reporter-Amplifier Architecture for Enhancing the Sensitivity of Molecular MRI by Water Exchange.

Journal

ChemBioChem, 25(10)

Authors

Huang, Yimeng

Chen, Xinyue

Zhu, Ziyue

et al.

Publication Date

2024-05-17

DOI

10.1002/cbic.202400087

Peer reviewed

HHS Public Access

Author manuscript

Chembiochem. Author manuscript; available in PMC 2024 November 29.

Published in final edited form as:

Chembiochem. 2024 May 17; 25(10): e202400087. doi:10.1002/cbic.202400087.

A Dual-gene Reporter-amplifier Architecture for Enhancing the Sensitivity of Molecular MRI by Water Exchange

Yimeng Huang[1], **Xinyue Chen**[2], **Ziyue Zhu**[2], **Arnab Mukherjee**[*,1,2,3]

[1]Department of Chemistry

[2]Department of Molecular, Cellular, and Developmental Biology

[3]Department of Chemical Engineering

Abstract

The development of genetic reporters for magnetic resonance imaging (MRI) is essential for investigating biological functions in vivo. However, current MRI reporters have low sensitivity, making it challenging to create significant contrast against the tissue background, especially when only a small fraction of cells express the reporter. To overcome this limitation, we developed an approach for amplifying the sensitivity of molecular MRI by combining a chemogenetic contrast mechanism with a biophysical approach to increase water diffusion through the co-expression of a dual-gene construct comprising an organic anion transporting polypeptide, Oatp1b3, and a water channel, Aqp1. We first show that the expression of Aqp1 amplifies MRI contrast in cultured cells engineered to express Oatp1b3. We demonstrate that the contrast amplification is caused by Aqp1-driven increase in water exchange, which provides the gadolinium ions internalized by Oatp1b3-expressing cells with access to a larger water pool compared with exchange-limited conditions. We further show that our methodology allows cells to be detected using approximately 10-fold lower concentrations of gadolinium than that in the Aqp1-free scenario. Finally, we show that our approach enables the imaging of mixed-cell cultures containing a low fraction of Oatp1b3-labeled cells that are undetectable on the basis of Oatp1b3 expression alone.

Keywords

reporter genes; MRI; aquaporins; Oatp1; diffusion

[*]Correspondence should be addressed to AM (arnabm@ucsb.edu).

Author Contributions

Yimeng Huang: Methodology, Investigation, Validation, Formal analysis, Writing - Review & Editing. **Xinyue Chen, Ziyue Zhu**: Investigation, Validation. **Arnab Mukherjee**: Conceptualization, Methodology, Formal analysis, Resources, Data Curation, Writing - Original Draft, Writing - Review & Editing, Visualization, Supervision, Project administration, Funding acquisition.

Conflicts of Interest

There are no conflicts to declare.

Supporting Information: The following files are available free of charge: “Huang et. al. SI 2023”. The file contains supplementary figures S1–S5, depicting the fluorescence distribution of CHO cells co-transduced with Oatp1b3 and Aqp1, diffusion and R_1 measurements of Aqp1 and Oatp1b3-expressing cells, estimation of intra-cellular gadolinium, R_1 enhancement by post-translational stabilization of Aqp1-FKBP12-DD using shield-1, detection of small fractions of Oatp1b3-labeled cells through Aqp1-driven R_1 enhancement, and Aqp1-driven R_1 enhancement of Gd-EOB-DTPA treated cells.

Introduction

Investigation of in vivo biological functions and the development of gene- and cell-based therapies require the use of reporter genes to track cellular and molecular events in intact organisms. Reporters that rely on optical excitation have limited utility in this context because of the absorption and scattering of light by biological tissues[1,2]. Consequently, efforts have been made to create reporter genes compatible with tissue-penetrant techniques such as nuclear[3–6], ultrasound[7–10], and magnetic resonance imaging (MRI)[11–23]. Among these techniques, MRI offers the most detailed three-dimensional views of tissues, organs, and organ systems, with a high spatial resolution and no exposure to ionizing radiation. These unique advantages have motivated numerous efforts to develop genetically encoded MRI reporters[24,25]. Most biomolecular reporters for MRI rely on proteins that interact with paramagnetic metals, such as iron[11–14,21,26], manganese[16,17,27], and gadolinium[23,28–30], to shorten the spin-lattice (T_1) and spin-spin relaxation times (T_2) of water molecules, allowing for the visualization of genetically labeled cells using T_1- and T_2-weighted imaging. In addition to paramagnetic relaxation, other mechanisms based on the diffusion of water molecules[20,22] and chemical exchange of protons[15,31–35] have also been explored. However, a major challenge for all classes of MRI reporter genes is their low sensitivity, which makes it difficult to create a significant contrast against the tissue background, especially when only a small population of cells expresses the reporter. This presents a significant obstacle in the application of MRI reporters to visualize biological processes such as neural activity, tumor metastasis, host-pathogen interactions, and cell trafficking, which often involve small numbers of reporter gene expressing cells.

To overcome the sensitivity limitations of current MRI reporters, we sought to develop an approach that combines paramagnetic relaxation enhancement with increased transmembrane water diffusion through the expression of two genetic constructs: an organic anion-transporting polypeptide, 1b3 (Oatp1b3), and a water channel, aquaporin-1 (Aqp1). Oatp1b3 is a hepatic drug transporter[36] that functions as an MRI reporter, because it facilitates the uptake of gadolinium ethoxybenzyl diethylenetriamine pentaacetic acid (Gd-EOB-DTPA)[37], a clinically approved contrast agent[23,28,38–40]. This results in shortening of the T_1 of water molecules within Oatp1b3-expressing cells, thereby enabling their visualization through T_1-weighted MRI (Fig. 1a). Aqp1, on the other hand, is a channel protein that facilitates the free and selective exchange of water molecules across the cell membrane and has been adapted as a reporter gene for visualizing cells using diffusion-weighted MRI[20,41] (Fig. 1b).

In order for Oatp1b3 to create contrast, the gadolinium centers that accumulate in Oatp1b3-expressing cells must be able to interact with water molecules. However, the native plasma membrane restricts water exchange, thereby limiting these paramagnetic interactions primarily to the water pool within Oatp1b3-expressing cells, and effectively excluding water in the extracellular volume and within surrounding cells that do not express Oatp1b3 (and therefore do not accumulate Gd-EOB-DTPA). This restriction of water access reduces effective paramagnetic relaxation enhancement, thereby limiting the minimum fraction of Oatp1b3-expressing cells that can be detected. We hypothesized that the expression of Aqp1 could overcome this limitation by providing Oatp1b3-expressing cells with access to a

larger water pool, thereby allowing more water molecules to contribute to T_1 relaxation compared to native conditions, where water exchange is limited by the native cell membrane (Fig. 1c). Because aquaporins enhance signals by permitting the unrestricted movement of water molecules across cellular boundaries, we refer to this mechanism as 'T_1-reporter visualization with increased sensitivity using aquaporins' (T_1-VISA) (Fig. 1c). Here, we describe the engineering and characterization of genetically encoded T_1-VISAs and demonstrate their efficacy in enhancing T_1 signals from mixed-cell populations containing low fractions of Oatp1b3-labeled cells that are otherwise undetectable based solely on reporter gene expression.

Results and Discussion

Aqp1 expression enhances the T_1-relaxation rate of Oatp1b3-expressing cells by facilitating water exchange

To test the feasibility of our concept, we co-transduced Chinese hamster ovary (CHO) cell lines with lentiviral vectors engineered to express Aqp1 and Oatp1b3. The expression of Oatp1b3 was driven by a constitutive promoter, EF1α, while Aqp1 was controlled by a minimal CMV promoter containing TetR-binding sites, allowing for inducible expression using doxycycline (Fig. 1d). An internal ribosome entry site (IRES) was employed to co-express each gene with a fluorescent reporter, allowing for the enrichment of doubly transduced cells by fluorescence-activated cell sorting (Supplementary Fig. 1). We confirmed that the doxycycline treatment resulted in an increase in diffusivity (Supplementary Fig. 2a) but produced no significant change in T_1 relaxation rate ($R_1 = 1/T_1$) (Supplementary Fig. 2b). In contrast, Oatp1b3 expression resulted in the expected increase in R_1 following the incubation of cells with the contrast agent, Gd-EOB-DTPA (Supplementary Fig. 2c). We then measured R_1 in cells co-expressing both Oatp1b3 and Aqp1 (Fig. 1d) and observed a marked increase in R_1 ($\Delta R_1/R_{1,\text{Aqp1-off}} = 43 \pm 3$ %, mean ± s.d., $P = 0.001$, $n = 6$, 2-sided t-test) compared to cells labeled with Oatp1b3 alone, i.e., without Aqp1 expression (Fig. 1e,f). To rule out the possibility that the increase in R_1 was driven by changes in the intracellular accumulation of Gd-EOB-DTPA, we used inductively coupled plasma atomic emission spectrometry (ICP-AES) to quantify gadolinium concentration, which showed that Oatp1b3-labeled cells accumulated comparable amounts of gadolinium in both Aqp1-on and off conditions (Supplementary Fig. 3).

Additionally, we investigated whether co-expressing Oatp1b3 and Aqp1 as a single transcript, i.e., under the same promoter, would result in a similar Aqp1-dependent increase in R_1. To modulate Aqp1 activity independently of Oatp1b3, we appended a destabilizing domain (DD) derived from the prolyl isomerase FKBP12 at the C-terminus of Aqp1. Our previous studies demonstrated that the Aqp1-FKBP12-DD fusion protein is constitutively destabilized, leading to a low-diffusivity off-state, but can be stabilized using a small-molecule, shield-1, which binds to the FKBP12-DD tag[42,43]. We incorporated both Oatp1b3 and Aqp1-FKBP12-DD in a single lentiviral vector separated by a ribosome-skipping 2A peptide sequence (Fig. 1g), created stable CHO cell lines by viral transduction, and performed R_1 measurements. In line with the increase in R_1 observed with doxycycline-

driven transcriptional induction of Aqp1, the modulation of Aqp1 at the post-translational level using shield-1 also results in a significant increase in R_1 ($\Delta R_1/R_{1,off}$ = 69.7 ± 1.3 %, P = 0.001) relative to cells that were not treated with shield-1 (Fig. 1h). Collectively, these findings demonstrate the viability of the T_1-VISAs methodology (Fig. 1c), which involves Aqp1 enhancing the paramagnetic relaxation of Oatp1b3-labeled cells by facilitating water exchange across the cell membrane.

Next, we examined the empirical relationship between the enhancement in water diffusivity mediated by Aqp1 ($\Delta D/D_{off}$) and the diffusion-dependent increase in relaxation rate ($\Delta R_1/R_{1,Aqp1\text{-}off}$). To this end, we utilized cells engineered to co-express Oatp1b3 in conjunction with doxycycline-inducible Aqp1 and varied the diffusion coefficient by altering the concentration of doxycycline administered to the cells. As before, we quantified the relative increase in R_1 compared to the baseline value obtained in the absence of Aqp1 expression. Our findings revealed that the increase in R_1 and diffusivity exhibit an approximately hyperbolic relationship, with $\Delta R_1/R_{1,Aqp1\text{-}off}$ tending to a plateau at high diffusion rates (Fig. 1i), suggesting a saturating fast-exchange regime in which the exchange rate of water molecules exceeds the Gd-EOB-DTPA induced increase in relaxation[44].

Aqp1 expression enables imaging using a lower concentration of contrast agent

The use of Oatp1b3 in biomedical applications requires a high dosage of Gd-EOB-DTPA to generate contrast (typically, 16 mM supplemented in growth media for in vitro imaging and >1 mmol/kg injected for in vivo applications[23,28,38–40,45]). Therefore, developing a strategy that enables Oatp1b3 to function effectively as an MRI reporter using a lower concentration of Gd-EOB-DTPA than the current experimental standard would be beneficial, particularly in situations where administering high doses of the contrast agent may be challenging or unsafe. Based on our findings above, we postulated that cells expressing both Oatp1b3 and Aqp1 could produce similar T_1 relaxation as Oatp1b3-only cells, but using a lower dosage of Gd-EOB-DTPA. To test this hypothesis, we incubated cells co-expressing Oatp1b3 and Aqp1 with varying concentrations of Gd-EOB-DTPA ranging from 1.6-16 mM and measured the relative increase in R_1 ($\Delta R_1/R_{1,Aqp1\text{-}off}$) compared to Oatp1b3-only cells treated with 16 mM Gd-EOB-DTPA. As expected, $\Delta R_1/R_{1,Aqp1\text{-}off}$ increased with increasing concentration of gadolinium (Fig. 2a). Notably, we found that co-expression of Oatp1b3 and Aqp1 allowed for an approximately 10-fold lower concentration of Gd-EOB-DTPA to achieve the same R_1 as cells expressing only Oatp1b3 (Fig. 2b).

Aqp1 enables detection of a small fraction of Oatp1b3-labeled cells in mixed populations

The ability to sensitively monitor small populations of genetically labeled cells is of great value in biomedical research. Therefore, we aimed to determine whether the exchange-based R_1 amplification provided by T_1-VISAs would enable the detection of small subsets of Oatp1b3-labeled cells in a mixed population consisting of both Oatp1b3-labeled and unlabeled cells (Fig. 3a). To this end, we prepared cell cultures containing varying fractions of Oatp1b3-labeled cells mixed with cells lacking Oatp1b3. Both cell types were engineered to express Aqp1 under the control of a doxycycline-inducible promoter, as previously described, thereby enabling acquisition of R_1 measurements in the presence and absence of uniform Aqp1 expression (Fig. 3a). As anticipated, R_1 increased with increasing Oatp1b3-

labeled cell fraction, both in the presence and absence of Aqp1 expression (Fig. 3b). However, R_1 values were consistently larger in the Aqp1-on population compared to the Aqp1-off population, as expected due to the increase in water exchange facilitated by Aqp1 expression (Fig. 3b). The amplification effect was lost when Aqp1 expression was switched off in Oatp1b3-expressing cells (by withholding doxycycline), further confirming that the increased access of Gd-EOB-DTPA within Oatp1b3-cells to water molecules is necessary to drive the increase in R_1 (Supplementary Fig. 4). Notably, this approach achieved a nearly 4-fold increase in R_1 even at low cell fractions (< 12 %) compared to Oatp1b3 alone i.e., without expression of Aqp1 (Fig. 3c). The resulting gain in sensitivity enabled the robust detection of as few as 3 % Oatp1b3-labeled cells ($\Delta R_1/R_{10}$ = 79 ± 9 %, P = 10^{-8}) that otherwise could not be detected with statistical significance based on Oatp1b3 expression alone ($\Delta R_1/R_{10}$ = 19 ± 3 %, P = 0.06) (Fig. 3d).

Conclusions

This study presents a novel dual gene reporter-amplifier architecture, named T_1-VISA, for highly sensitive detection of genetically labeled cells using MRI. While previous research has demonstrated the amplification of T_1 signals through the modulation of lipid bilayer permeability in the context of liposomes[46–48] and MR thermometry[49,50], the current study introduces the first fully genetic approach for exchange-based signal amplification in molecular MRI. The methodology utilizes Aqp1 and Oatp1b3, two genes that have proven effective as standalone reporters in various in vivo applications, including monitoring transcriptional activity[28,51,52], detecting metastases[38], tracking cell-cell communication[40], and examining neural activity and connectivity within the mouse brain[53,54]. Compared to Oatp1b3 utilized alone, T_1-VISA demonstrated a substantial improvement in detection sensitivity, with the ability to detect on the order of 10^3 cells per voxel. Notably, Oatp1b3 has shown success in detecting lesions estimated to comprise a few thousand cells in vivo[38]. Therefore, we anticipate that the T_1-VISA methodology has the potential to achieve a detection limit on the order of a few hundred cells per voxel, which is among the highest sensitivity achieved by any genetic material for MRI to our knowledge. Furthermore, the ability to generate contrast with reduced gadolinium doses may be particularly beneficial in expanding the use of Oatp1b3 in applications where administering a large amount of contrast agent is difficult, such as for imaging in the intact brain when the reagent needs to cross the blood-brain barrier (BBB)[54].

Initial applications of T_1-VISAs would likely involve the localized delivery of viral vectors encoding Aqp1 expression from a constitutive promoter and Oatp1b3 from an inducible promoter to respectively allow exchange-based amplification and monitoring of transcription factor activity. However, future applications of T_1-VISAs could greatly benefit from advances in gene delivery techniques and transgenic models, which would enable the homogeneous organ-wide expression of Aqp1 to be seamlessly integrated with the expression of Oatp1b3 from promoters that reporter on cell fate, signaling pathways, and other biological functions.

In addition to the anticipated in vivo applications, future research on T_1-VISAs could explore the use of alternative Oatp1 variants and gadolinium-or manganese-based contrast

agents[55,56] to further enhance sensitivity and lower the contrast agent dosage. Additionally, the Aqp1-based mechanism for enhancing relaxation is not exclusive to Oatp1b3, and can be adapted to improve the performance of other classes of metal-based MRI reporters, most of which have similarly limited sensitivity. Furthermore, this approach could be used to amplify the fairly weak signal changes observed with secreted or extracellularly localized MRI reporters, such as those designed to detect neurotransmitters[57,58] and enzyme activity[29]. Preliminary results from our lab suggest that Aqp1 expression can significantly increase the relaxation rate of cells supplemented with Gd-EOB-DTPA in the extracellular volume (Supplementary Fig. 5), which establishes the conceptual feasibility of using Aqp1 to amplify the relaxation enhancement induced by extracellular reporters and contrast agents. Moreover, the ability to precisely tune water diffusion using Aqp1 could offer a way to experimentally test and refine biophysical models of contrast agent relaxation, such as those based on the Bloch-McConnel-Woessner equations, which are essential for accurate interpretation of dynamic contrast-enhanced MRI in perfusion imaging. Finally, T_1-VISAs can be harnessed to create a new class of MRI reporters for functional imaging by using aquaporin variants that regulate membrane trafficking or diffusion through the channel pore in response to biological analytes, such as calcium, pH, and enzyme activity.

In summary, we anticipate that the development of T_1-VISAs will open up new avenues of scientific exploration in fields such as systems neuroscience, immuno-oncology, and in vivo synthetic biology where highly sensitive deep-tissue reporters are eagerly sought after for tracking biological functions in small and large animals. In practical terms, the development of T_1-VISAs will also complement advances in gene therapies and cell-based medicine, where the ability to monitor these therapies in animals with high sensitivity will be critical to their clinical translation.

Methods

Molecular biology

The DNA sequences encoding Oatp1b3 (Addgene plasmid #132200), Aqp1, and Aqp1-FKBP12-DD were amplified using Q5® High-Fidelity 2X Master Mix (New England Biolabs, Ipswich, MA, USA) and cloned by Gibson assembly in a lentiviral transfer vector under the control of a constitutive promoter, EF1α (Addgene plasmid #60058) or a doxycycline-inducible minimal CMV promoter (Addgene plasmid #26431). EGFP and tdTomato were co-expressed with Aqp1 and Oatp1b3 respectively using an internal ribosome entry site (IRES) to facilitate the selection of stably transduced cells by fluorescence-activated cell sorting (FACS). FLAG and hemagglutinin (HA) epitope tags were added at the N-termini of Aqp1 and Oatp1b3 respectively to facilitate their detection by Western blotting, using anti-FLAG and anti-HA antibodies. The integrity all constructs was confirmed by Sanger sequencing (Genewiz, San Diego, CA, USA) or whole-plasmid nanopore sequencing (Plasmidsaurus, Eugene, OR, USA).

Construction and packaging of lentivirus

The packaging of lentivirus was accomplished using a three-plasmid system consisting of a packaging plasmid, an envelope plasmid encoding VSV-G (to confer broad tropism), and

the transfer plasmids constructed above. The three plasmids were combined in a ratio of 22 μg each for the packaging and transfer plasmids, and 4.5 μg for the envelope plasmid, and delivered to HEK293T cells by transient transfection using linear 25 kDa polyethyleneimine (Polysciences). About 24 h post-transfection, the cells were treated with sodium butyrate (10 mM) to stimulate viral gene expression. Approximately 72 h post-transfection, the supernatant was harvested and centrifuged at 500 x g for 10 min to remove cell debris. The cleared supernatant was then mixed with Lenti-X Concentrator (Takara Bio) and incubated for 24 h at 4 °C. Finally, the mixture was centrifuged at 1500 x g for 45 min at 4 °C to precipitate lentivirus. The resulting viral particles were resuspended in 0.2 mL Dulbecco's Modified Eagle Medium (DMEM) and either immediately used for transduction of CHO cells or stored as single-use aliquots at −80 °C.

Mammalian cell engineering

CHO cells were routinely cultured in 10-cm tissue culture grade plates using high-glucose DMEM supplemented with 10 % fetal bovine serum (R&D systems, Bio-Techne), 110 μg/mL sodium pyruvate, 100 U/mL penicillin, and 100 μg/mL streptomycin (Thermo Fisher Scientific, Waltham, MA, USA), and housed in a humidified incubator at 37 °C and 5 % CO_2. In preparation for lentiviral transduction, CHO cells were grown to 70-80 % confluency in six-well plates, aspirated to remove spent media, and treated with purified viral particles resuspended in 0.8 mL DMEM containing 8 μg/mL polybrene (Thermo Fisher Scientific). The cells were spinfected by centrifuging the six-well plates at 1050 x g for 90 min at 30 °C and the returned to the 37 °C incubator for another 48 h. Stably transduced cells were selected by FACS using a Sony MA900 sorter and stored as cryo-stocks in the vapor phase of liquid nitrogen.

Inductively coupled plasma atomic emission spectrometry

Following incubation of cells with Gd-EOB-DTPA for 90 min, the media was aspirated and cells were washed with sterile PBS. The cells were then treated with 0.25 % trypsin-EDTA to detach from the surface, and centrifuged at 350 x g for 5 min. The cells were washed with sterile PBS an additional 5 times, and then approximately 5 x 10^6 cells (determined by cell counting using a C-chip™ disposable hemocytometer, Fisher Scientific) were lysed using 0.5 ml RIPA lysis buffer (Santa Cruz Biotech, Dallas, TX). Subsequently, 2 mL of 70 % (v/v) concentrated nitric acid (Fisher Scientific) was added to each sample, stirred, and heated carefully on a hot plate for approximately 24 h, inside a fume hood. After this, 1 mL of 30 % hydrogen peroxide solution (Fisher Scientific) was added to each sample, stirred, and further heated on hot plate for ~ 24 h in a fume hood until the sample solution appeared clear and colorless. Each sample was then diluted using deionized water to reach a final concentration of 10% (v/v) nitric acid. The gadolinium concentrations in the ensuing samples were determined by Thermo iCAP 6300 Inductively coupled plasma atomic emission spectrometer (ICP-AES), using serial dilutions of a gadolinium ICP standard (Inorganic Ventures, Avantor™) for calibration.

Magnetic resonance imaging

Whole-cell MRI measurements were performed using cell pellets, as described in our previous studies[20,41,59,60]. Briefly, prior to undergoing MRI, cells were seeded in in 10

cm tissue culture plates such that they reached confluence within approximately 48 h from the time of seeding. For cells harboring an inducible Aqp1 construct, doxycycline hyclate (0.01-1 μg/mL) was added to the culture media approximately 24 h after seeding. For cells harboring the Aqp1-FKBP12-DD construct, shield-1 (1 μM) was added to the culture media approximately 24 h after seeding. Cells were then incubated with Gd-EOB-DTPA (Eovist®, Bayer HealthCare, Germany) at concentrations ranging from 1.6-16 mM for 90 minutes before being detached from the surface by treatment with 0.25 % trypsin-EDTA (Thermo Fisher Scientific). The detached cells were then centrifuged at 350 x g for 5 minutes, washed three times with sterile phosphate buffered saline (PBS), and resuspended in 0.2 mL of sterile PBS in 0.2 plastic PCR tubes. For experiments involving mixtures of cells with and without Oatp1b3 expression, the two cell types were separately cultured and harvested as described above. The cell density was determined by cell counting using a hemocytometer, and the appropriate number of cells from each culture were mixed by gentle pipetting to achieve a desired proportion of Oatp1b3-expressing cells in the mixture. The mixed cell suspension was then centrifuged at 350 x g for 5 minutes, washed three times with sterile PBS, and transferred to 0.2 mL plastic tubes. The tubes containing the resuspended cells were centrifuged at 500 x g for 5 minutes to form a cell pellet and placed in water-filled agarose (1% w/v) molds housed in a 3D-printed MRI phantom. The final pellet (~ 20 μL) used for whole-cell relaxometry and diffusion measurements comprised approximately 5×10^6 cells, corresponding to ~ 10^5 cells per unit voxel (0.04 μL).

All MR imaging experiments were performed in a Bruker 7T vertical-bore MRI scanner using a 66 mm diameter transceiver coil. The cell pellets were first located using a fast low angle shot (FLASH) localizer scan with the following parameters: echo time, T_E = 3 ms, repetition time, T_R = 100 ms, flip angle, α = 30 degrees, matrix size = 128 × 128, field of view (FOV) = 4.5 × 4.5 cm^2, slice thickness = 2 mm, number of averages = 1, and total acquisition time = 12.8 s. Subsequently, a series of T_1-weighted scans were acquired in the axial plane using a rapid acquisition with refocused echoes (RARE) pulse sequence, with the following parameters: T_E = 5.3 ms, flip angle, α = 90 degrees, matrix size = 128 × 128, FOV = 5.6 × 5.6 cm^2, slice thickness = 2 mm, number of averages = 4, RARE factor = 8, total acquisition time =13 min, and variable T_R = 53, 170, 302.5, 455, 635, 855, 1138, 1533, 2195, and 5000 ms. To measure cellular water diffusivity, we acquired diffusion-weighted images of cell pellets in the axial plane using a stimulated echo pulse sequence with the following parameters: T_E = 18 ms, T_R = 1000 ms, gradient duration, δ = 5 ms, gradient separation, Δ = 300 ms, matrix size = 128 × 128, FOV = 4.5 × 4.5 cm^2, slice thickness = 2 mm, number of averages = 5, 4 effective b-values = 1115, 1794, 2294, 2794 s/mm^2, and total acquisition time = 42 min. All images were acquired using ParaVision 6 (Bruker) and stored as DICOM files, and were analyzed using Fiji or ImageJ (National Institutes of Health). The signal intensity at a given b-value or repetition time was estimated by computing the average intensity of all voxels inside a manually drawn region of interest (ROI) encompassing the axial cross section view of a cell pellet. The relaxation time (T_1) was calculated by fitting the growth of mean signal intensity as a function of T_R to an exponential function. The apparent diffusion coefficient (D) was calculated from the slope of the exponential decay in mean signal intensity as a function of effective b-value. Least-squares regression fitting was performed using the fitnlm function in Matlab (R2022b).

Statistical analysis

Data are summarized by their mean and standard deviation obtained from $n \geq 3$ independent biological replicates. All MRI measurements were obtained using the same batch of lentivirally transduced stable cell lines. Each biological replicate refers to cells that were individually passaged in separate plates, with a maximum of two independent plates being measured on the same day. Hypothesis testing is performed using the Student's t-test. All tests are 2-sided and P value < 0.05 taken to indicate statistical significance. Quality of model-fitting (to estimate diffusivity) was ascertained based on the regression coefficient.

Supplementary Material

Refer to Web version on PubMed Central for supplementary material.

Acknowledgements

We thank members of the Mukherjee lab for helpful discussions. Dr. Jerry Hu (UC, Santa Barbara) is gratefully acknowledged for assistance with setting up the MRI workflow. This research was supported by the National Institutes of Health (R35-GM133530, R21-EB033989, and R01-NS128278 to A.M.). This project has been made possible in part by a grant from the Chan Zuckerberg Initiative DAF, an advised fund of Silicon Valley Community Foundation. All MRI experiments were performed at the Materials Research Laboratory (MRL) at UC, Santa Barbara. The MRL Shared Experimental Facilities are supported by the MRSEC Program of the NSF under Award No. DMR 1720256; a member of the NSF-funded Materials Research Facilities Network.

Data availability.

The data that support the findings of this study are available from the corresponding author upon reasonable request.

References

[1]. Helmchen F, Denk W, Nat Methods 2005, 2, 932–940. [PubMed: 16299478]

[2]. Ntziachristos V, Nat Methods 2010, 7, 603–614. [PubMed: 20676081]

[3]. Yaghoubi SS, Campbell DO, Radu CG, Czernin J, Theranostics 2012, 2, 374–391. [PubMed: 22509201]

[4]. Minn I, Huss DJ, Ahn H-H, Chinn TM, Park A, Jones J, Brummet M, Rowe SP, Sysa-Shah P, Du Y, Levitsky HI, Pomper MG, Science Advances 2019, 5, eaaw5096. [PubMed: 31281894]

[5]. Sellmyer MA, Richman SA, Lohith K, Hou C, Weng C-C, Mach RH, O'Connor RS, Milone MC, Farwell MD, Molecular Therapy 2020, 28, 42–51. [PubMed: 31668558]

[6]. Keu KV, Witney TH, Yaghoubi S, Rosenberg J, Kurien A, Magnusson R, Williams J, Habte F, Wagner JR, Forman S, Brown C, Allen-Auerbach M, Czernin J, Tang W, Jensen MC, Badie B, Gambhir SS, Sci Transl Med 2017, 9, eaag2196. [PubMed: 28100832]

[7]. Farhadi A, Sigmund F, Westmeyer GG, Shapiro MG, Nat. Mater 2021, 20, 585–592. [PubMed: 33526879]

[8]. Farhadi A, Ho GH, Sawyer DP, Bourdeau RW, Shapiro MG, Science 2019, 365, 1469–1475. [PubMed: 31604277]

[9]. Bourdeau RW, Lee-Gosselin A, Lakshmanan A, Farhadi A, Kumar SR, Nety SP, Shapiro MG, Nature 2018, 553, 86–90. [PubMed: 29300010]

[10]. Hurt RC, Buss MT, Duan M, Wong K, You MY, Sawyer DP, Swift MB, Dutka P, Barturen-Larrea P, Mittelstein DR, Jin Z, Abedi MH, Farhadi A, Deshpande R, Shapiro MG, Nat Biotechnol 2023, 1–13. [PubMed: 36653493]

[11]. Genove G, DeMarco U, Xu H, Goins WF, Ahrens ET, Nat Med 2005, 11, 450–454. [PubMed: 15778721]

[12]. Iordanova B, Ahrens ET, NeuroImage 2012, 59, 1004–1012. [PubMed: 21939774]

[13]. Cohen B, Ziv K, Plaks V, Israely T, Kalchenko V, Harmelin A, Benjamin LE, Neeman M, Nat Med 2007, 13, 498–503. [PubMed: 17351627]

[14]. Cohen B, Dafni H, Meir G, Harmelin A, Neeman M, Neoplasia 2005, 7, 109–117. [PubMed: 15802016]

[15]. Gilad AA, McMahon MT, Walczak P, Winnard PT, Raman V, van Laarhoven HWM, Skoglund CM, Bulte JWM, van Zijl PCM, Nat Biotechnol 2007, 25, 217–219. [PubMed: 17259977]

[16]. Bartelle BB, Szulc KU, Suero-Abreu GA, Rodriguez JJ, Turnbull DH, Magnetic Resonance in Medicine 2013, 70, 842–850. [PubMed: 23065715]

[17]. Bartelle BB, Mana MD, Suero-Abreu GA, Rodriguez JJ, Turnbull DH, Magnetic Resonance in Medicine 2015, 74, 1750–1757. [PubMed: 25522343]

[18]. Bartelle BB, Berríos-Otero CA, Rodriguez JJ, Friedland AE, Aristizábal O, Turnbull DH, Circulation Research 2012, 110, 938–947. [PubMed: 22374133]

[19]. Ghosh S, Li N, Schwalm M, Bartelle BB, Xie T, Daher JI, Singh UD, Xie K, DiNapoli N, Evans NB, Chung K, Jasanoff A, Nat Neurosci 2022, 25, 390–398. [PubMed: 35241803]

[20]. Mukherjee A, Wu D, Davis HC, Shapiro MG, Nat Commun 2016, 7, 13891. [PubMed: 28008959]

[21]. Patrick PS, Rodrigues TB, Kettunen MI, Lyons SK, Neves AA, Brindle KM, Magnetic Resonance in Medicine 2016, 75, 1697–1707. [PubMed: 25981669]

[22]. Schilling F, Ros S, Hu D-E, D'Santos P, McGuire S, Mair R, Wright AJ, Mannion E, Franklin RJM, Neves AA, Brindle KM, Nat Biotechnol 2017, 35, 75–80. [PubMed: 27918546]

[23]. Patrick PS, Hammersley J, Loizou L, Kettunen MI, Rodrigues TB, Hu D-E, Tee S-S, Hesketh R, Lyons SK, Soloviev D, Lewis DY, Aime S, Fulton SM, Brindle KM, Proceedings of the National Academy of Sciences 2014, 111, 415–420.

[24]. Brindle KM, Trends in Genetics 2022, 38, 996–998. [PubMed: 35641343]

[25]. Gilad AA, Ziv K, McMahon MT, van Zijl PCM, Neeman M, Bulte JWM, Journal of Nuclear Medicine 2008, 49, 1905–1908. [PubMed: 18997049]

[26]. Deans AE, Wadghiri YZ, Bernas LM, Yu X, Rutt BK, Turnbull DH, Magnetic Resonance in Medicine 2006, 56, 51–59. [PubMed: 16724301]

[27]. Szulc DA, Lee XA, Cheng H-YM, Cheng H-LM, iScience 2020, 23, DOI 10.1016/j.isci.2020.101350.

[28]. Kelly JJ, Saee-Marand M, Nyström NN, Evans MM, Chen Y, Martinez FM, Hamilton AM, Ronald JA, Science Advances 2021, 7, eabc3791. [PubMed: 33523917]

[29]. Taghian T, Batista AR, Kamper S, Caldwell M, Lilley L, Li H, Rodriguez P, Mesa K, Zheng S, King RM, Gounis MJ, Todeasa S, Maguire A, Martin DR, Sena-Esteves M, Meade TJ, Gray-Edwards HL, Molecular Therapy - Methods & Clinical Development 2021, 23, 128–134. [PubMed: 34703836]

[30]. Louie AY, Hüber MM, Ahrens ET, Rothbächer U, Moats R, Jacobs RE, Fraser SE, Meade TJ, Nat Biotechnol 2000, 18, 321–325. [PubMed: 10700150]

[31]. Bar-Shir A, Liu G, Chan KWY, Oskolkov N, Song X, Yadav NN, Walczak P, McMahon MT, van Zijl PCM, Bulte JWM, Gilad AA, ACS Chem. Biol 2014, 9, 134–138. [PubMed: 24138139]

[32]. Allouche-Arnon H, Khersonsky O, Tirukoti ND, Peleg Y, Dym O, Albeck S, Brandis A, Mehlman T, Avram L, Harris T, Yadav NN, Fleishman SJ, Bar-Shir A, Nat Biotechnol 2022, 40, 1143–1149. [PubMed: 35102291]

[33]. Minn I, Bar-Shir A, Yarlagadda K, Bulte JWM, Fisher PB, Wang H, Gilad AA, Pomper MG, Magnetic Resonance in Medicine 2015, 74, 544–549. [PubMed: 25919119]

[34]. Bar-Shir A, Bulte JWM, Gilad AA, ACS Chem. Biol 2015, 10, 1160–1170. [PubMed: 25730583]

[35]. Bricco AR, Miralavy I, Bo S, Perlman O, Korenchan DE, Farrar CT, McMahon MT, Banzhaf W, Gilad AA, ACS Synth. Biol 2023, 12, 1154–1163. [PubMed: 36947694]

[36]. Pan Q, Zhu G, Xu Z, Zhu J, Ouyang J, Tong Y, Zhao N, Zhang X, Cheng Y, Zhang L, Tan Y, Li J, Zhang C, Chen W, Cai S-Y, Boyer JL, Chai J, Cellular and Molecular Gastroenterology and Hepatology 2023, 16, 223–242. [PubMed: 37146714]

[37]. Van Beers BE, Pastor CM, Hussain HK, Journal of Hepatology 2012, 57, 421–429. [PubMed: 22504332]

[38]. Nyström NN, McRae SW, Martinez FM, Kelly JJ, Scholl TJ, Ronald JA, Cancer Research 2023, 83, 673–685. [PubMed: 36512633]

[39]. Nyström NN, Hamilton AM, Xia W, Liu S, Scholl TJ, Ronald JA, Invest Radiol 2019, 54, 302–311. [PubMed: 30672844]

[40]. Wang T, Chen Y, Nystrom NN, Liu S, Fu Y, Martinez FM, Scholl TJ, Ronald JA, Proceedings of the National Academy of Sciences 2023, 120, e2216901120.

[41]. Chowdhury R, Wan J, Gardier R, Rafael-Patino J, Thiran J-P, Gibou F, Mukherjee A, ACS Synth. Biol 2023, 12, 3041–3049. [PubMed: 37793076]

[42]. Yun J, Baldini L, Huang Y, Li E, Li H, Chacko AN, Miller ADC, Wan J, Mukherjee A, bioRxiv [Preprint] 2023, 2023.06.02.543364.

[43]. Banaszynski LA, Chen L, Maynard-Smith LA, Ooi AGL, Wandless TJ, Cell 2006, 126, 995–1004. [PubMed: 16959577]

[44]. Lee J-H, Springer CS Jr., Magnetic Resonance in Medicine 2003, 49, 450–458. [PubMed: 12594747]

[45]. Bhattacharyya T, Mallett CL, Hix JM-L, Shapiro EM, 2023, 2023.08.07.552326.

[46]. Simon J, Schwalm M, Morstein J, Trauner D, Jasanoff A, Nat. Biomed. Eng 2023, 7, 313–322. [PubMed: 36550300]

[47]. Fossheim SL, Fahlvik AK, Klaveness J, Muller RN, Magnetic Resonance Imaging 1999, 17, 83–89. [PubMed: 9888401]

[48]. Koenig SH, Ahkong QF, Brown RD 3rd, Lafleur M, Spiller M, Unger E, Tilcock C, Magnetic Resonance in Medicine 1992, 23, 275–86 [PubMed: 1549042]

[49]. Fossheim SL, Il'yasov KA, Hennig J, Bjørnerud A, Acad Radiol 2000, 7, 1107–1115. [PubMed: 11131055]

[50]. Lindner LH, Reinl HM, Schlemmer M, Stahl R, Peller M, Int J Hyperthermia 2005, 21, 575–588. [PubMed: 16147441]

[51]. Zhang L, Gong M, Lei S, Cui C, Liu Y, Xiao S, Kang X, Sun T, Xu Z, Zhou C, Zhang S, Zhang D, Eur J Nucl Med Mol Imaging 2022, 49, 2310–2322. [PubMed: 35044495]

[52]. Li M, Liu Z, Wu Y, Zheng N, Liu X, Cai A, Zheng D, Zhu J, Wu J, Xu L, Li X, Zhu L-Q, Manyande A, Xu F, Wang J, Mol Psychiatry 2022, 1–8.

[53]. Zheng N, Li M, Wu Y, Kaewborisuth C, Li Z, Gui Z, Wu J, Cai A, Lin K, Su K-P, Xiang H, Tian X, Manyande A, Xu F, Wang J, NeuroImage 2022, 258, 119402. [PubMed: 35732245]

[54]. Li S, Xu X, Li C, Xu Z, Wu K, Ye Q, Zhang Y, Jiang X, Cang C, Tian C, Wen J, NeuroImage 2023, 281, 120374. [PubMed: 37729795]

[55]. Nyström NN, Liu H, Martinez FM, Zhang X, Scholl TJ, Ronald JA, J. Med. Chem 2022, 65, 9846–9857.

[56]. McRae SW, Cleary M, DeRoche D, Martinez FM, Xia Y, Caravan P, Gale EM, Ronald JA, Scholl TJ, J. Med. Chem 2023, 66, 6567–6576. [PubMed: 37159947]

[57]. Hai A, Cai LX, Lee T, Lelyveld VS, Jasanoff A, Neuron 2016, 92, 754–765. [PubMed: 27773583]

[58]. Shapiro MG, Westmeyer GG, Romero PA, Szablowski JO, Küster B, Shah A, Otey CR, Langer R, Arnold FH, Jasanoff A, Nat Biotechnol 2010, 28, 264–270. [PubMed: 20190737]

[59]. Ozbakir HF, Miller ADC, Fishman KB, Martins AF, Kippin TE, Mukherjee A, ACS Sens. 2021, 6, 3163–3169. [PubMed: 34420291]

[60]. Borg RE, Ozbakir HF, Xu B, Li E, Fang X, Peng H, Chen IA, Mukherjee A, Sens. Diagn 2023, 2, 948–955. [PubMed: 38405385]

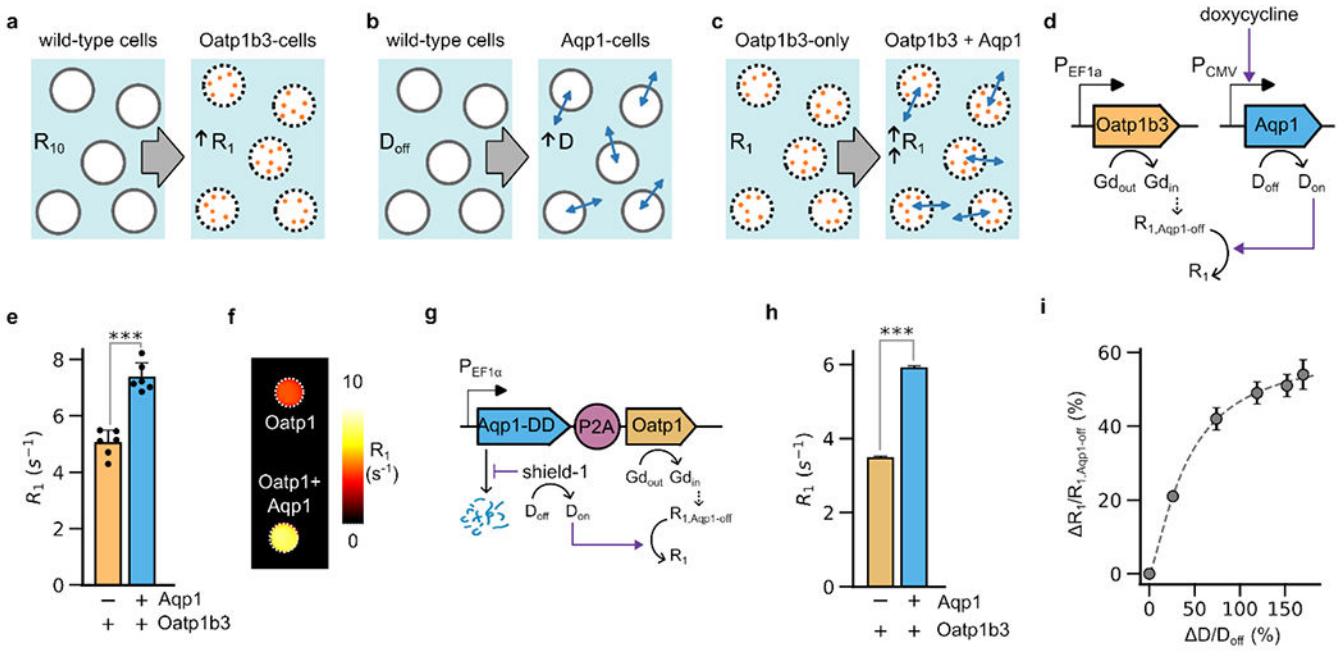

Figure 1: Aqp1-driven enhancement of T_1 relaxation.

(a) Illustration depicting the increase in the baseline T_1 relaxation rate (R_{10}) of cells (white circles) due to the expression of Oatp1b3, which promotes the intracellular uptake of Gd-EOB-DTPA (depicted as light brown, filled circles). The baseline T_1 relaxation rate (R_{10}) refers to the cellular relaxation rate in the absence of contrast agents. **(b)** Illustration depicting the increase in the baseline diffusivity of cells (D_0) due to expression of Aqp1, which facilitates transmembrane water exchange (depicted by bidirectional blue arrows). **(c)** Illustration depicting the increase in R_1 of Oatp1b3-expressing cells due to co-expression of Aqp1, which permits intracellular Gd-EOB-DTPA to access a larger pool of water molecules via transmembrane exchange. **(d)** Schematic outline of the T_1-VISA mechanism, which incorporates a constitutively expressed reporter gene (Oatp1b3) that promotes the uptake of Gd-EOB-DTPA; and an amplifier gene (Aqp1) that can be induced with doxycycline to enhance diffusivity ($D_{on} > D_{off}$) and consequently elevate the T_1-relaxation rate of cells relative to conditions where Aqp1 expression is not induced ($R_1 > R_{1,Aqp1\text{-}off}$). **(e)** T_1 relaxation rate ($R_1 = 1/T_1$) of Oatp1b3-expressing cells in the absence and presence of Aqp1 expression modulated by withholding or adding doxycycline. **(f)** R_1 maps of Oatp1b3-labeled cells in the absence and presence of Aqp1 expression. **(g)** Schematic representation of genetic construct engineered to co-express Oatp1b3 and Aqp1 as a single transcript. Aqp1 is tagged with a destabilizing domain (DD) derived from FKBP12F36V/L106P, which permits post-translational modulation of Aqp1 concentration by treatment with shield-1, a small-molecule that binds to the DD and stabilizes the Aqp1-FKBP12-DD fusion. **(h)** R_1 of CHO cells stably transduced to express the single-transcript Aqp1-FKBP12-DD construct with and without stabilization of Aqp1 through shield-1 treatment. **(i)** Increase in the T_1 relaxation rate ($\Delta R_1/R_{1,Aqp1\text{-}off}$) of Oatp1b3-labeled cells as a function of change in diffusivity ($\Delta D/D_{off}$). To alter diffusivity, cells were treated with varying concentrations of doxycycline in the range of 0.01-1 μg/mL, which induces different levels of Aqp1 expression from the minimal CMV promoter. The dotted line represents a hyperbolic fit

to the experimental data and is included to aid in the visual tracking of the trend in $\Delta R_1/R_{1,Aqp1\text{-}off}$ vs. $\Delta D/D_{off}$. The diffusivity and relaxation measurements were conducted at ambient temperature at a field strength of 7 Tesla. Each MRI measurement was obtained from a 2 mm thick axial section through a pellet formed by centrifuging a suspension of approximately 5×10^6 cells harvested from one confluent 10 cm tissue culture dish, which corresponds to approximately 10^5 cells per unit voxel (~ 0.4 μL). Error bars represent standard deviation from n ≥ 3 biological replicates. *** P-value < 0.001.

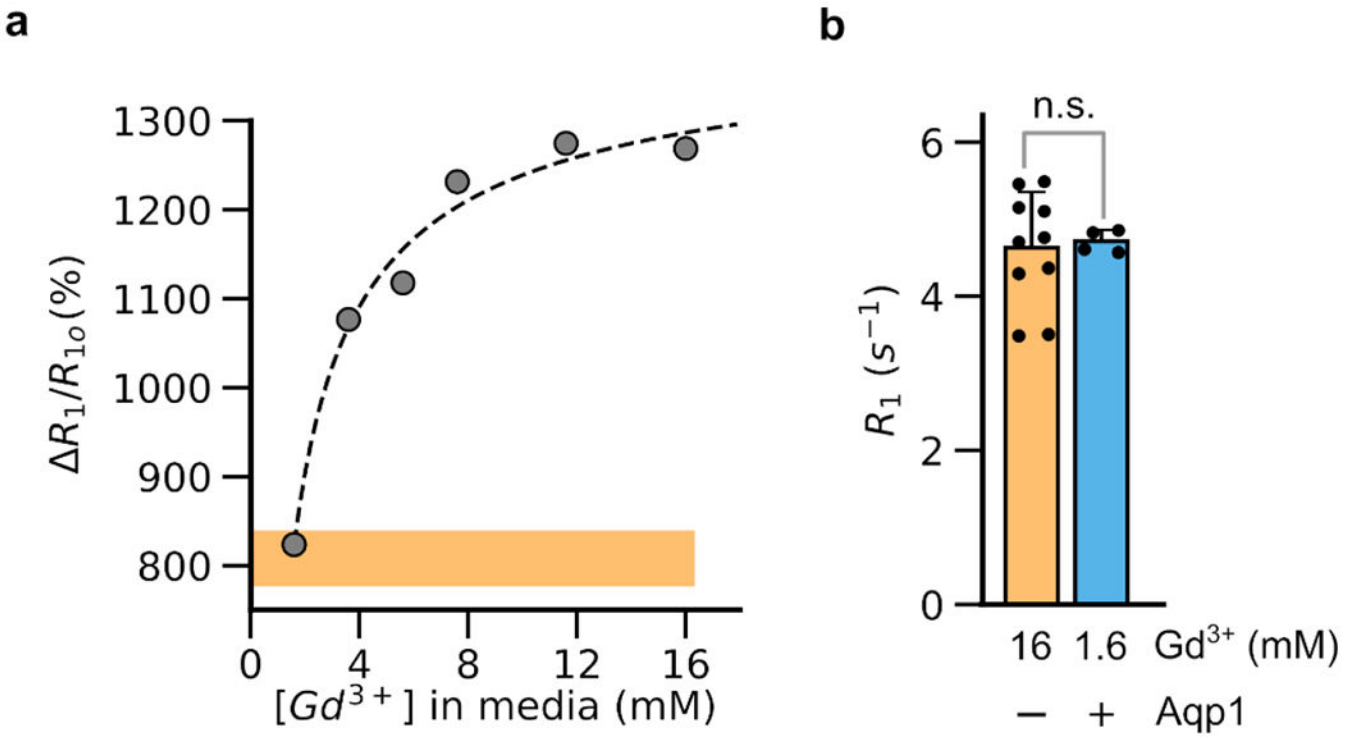

Figure 2: Effect of contrast agent concentration on T_1 relaxation.

(a) Percentage increase in R_1 of Oatp1b3-labeled CHO cells relative to unlabeled cells ($\Delta R_1/R_{10}$) as a function of Gd-EOB-DTPA concentration in the presence of Aqp1 expression. The dotted line represents a hyperbolic fit to the experimental data and is included to aid in the visual tracking of the trend in $\Delta R_1/R_{10}$ vs. gadolinium. The orange band indicates the 95 % confidence interval of the increase in R_1 ($\Delta R_1/R_{10}$) obtained without Aqp1 expression following the incubation of cells with 16 mM Gd-EOB-DTPA. The baseline T_1 relaxation rate (R_{10}) is the cellular relaxation rate measured in the absence of contrast agents. **(b)** R_1 of Oatp1b3-expressing cells with and without Aqp1 co-expression after incubation with 16 mM or 1.6 mM Gd-EOB-DTPA. Cells were incubated with the indicated Gd-EOB-DTPA concentration for 90 minutes, washed, and prepared for MRI as described in Methods. Diffusivity and relaxation measurements were conducted at ambient temperature at a field strength of 7 Tesla. Each MRI measurement was obtained from a 2 mm thick axial section through a pellet formed by centrifuging a suspension of approximately 5×10^6 cells harvested from one confluent 10 cm tissue culture dish, which corresponds to approximately 10^5 cells per unit voxel (~ 0.4 μL). Error bars represent the standard deviation from $n \geq 3$ biological replicates. In (a), the error bars are smaller than the data markers. n.s. P-value ≥ 0.05.

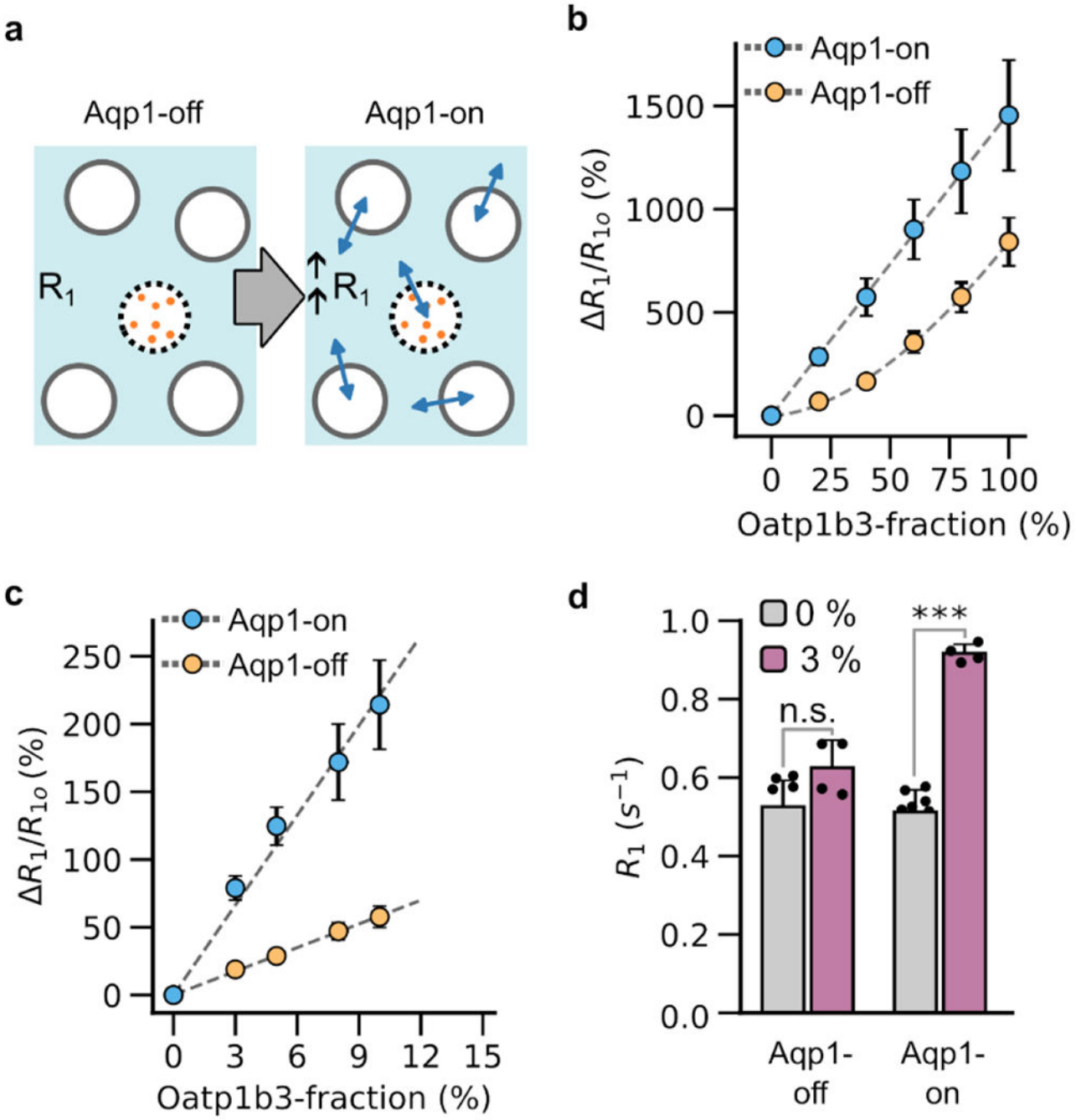

Figure 3: Detection of small fractions of Oatp1b3-labeled cells in mixed populations via Aqp1-driven enhancement in R_1.

(a) Illustration depicting a mixed-cell configuration comprising Oatp1b3-labeled cells (dotted circles with internalized Gd-EOB-DTPA labeled as filled light brown circles) and cells lacking Oatp1b3 (white circles). In the Aqp1-on state, all cells uniformly express Aqp1, enabling the amplification of R_1 through enhanced water exchange. **(b)** Percentage increase in R_1 ($\Delta R_1/R_{10}$) of mixed-cell populations comprising varying fractions (20, 40, 60, 80, and 100 %) of Oatp1b3-labeled cells relative to an identically prepared cell

population containing no Oatp1b3-labeled cells. Aqp1 expression was either off or induced by incubating cells with doxycycline. The baseline T_1 relaxation rate (R_{10}) is the cellular relaxation rate measured in the absence of contrast agents. The dotted line represents an empirical fit to the experimental data and is included to aid in the visual tracking of the trend in $\Delta R_1 / R_{10}$ vs. Oatp1b3-labeled cell fraction. **(c)** The percentage change in R_1 of mixed-cell populations comprising low fractions of Oatp1b3-labeled cells (0-15 %) relative to a cell population containing no Oatp1b3-labeled cells in the presence or absence of Aqp1 expression. The dotted lines represent linear fits to the experimental data and are included to aid in the visual tracking of the functional trend in $\Delta R_1/R_{10}$ vs. the Oatp1b3-labeled cell fraction. **(d)** R_1 of mixed-cell populations comprising 3 % Oatp1b3-labeled cells and a population containing no Oatp1b3-labeled cells in the presence and absence of Aqp1 expression. Relaxation measurements were conducted at ambient temperature at 7 Tesla. Each MRI measurement was obtained from a 2 mm thick axial section through a pellet formed by centrifuging a suspension of approximately 5×10^6 cells harvested from one confluent 10 cm tissue culture dish, which corresponds to approximately 10^5 cells per unit voxel (~ 0.4 μL). Error bars represent the standard deviation from $n \geq 3$ biological replicates and are smaller than the data markers in some cases. *** P-value < 0.001; n.s. P-value ≥ 0.05.